Role of a higher-dimensional interaction in stabilizing charge density waves in quasi-one-dimensional $NbSe_3$ revealed by angle-resolved photoemission spectroscopy

C. W. Nicholson,[1,*] E. F. Schwier,[2] K. Shimada,[2] H. Berger,[3] M. Hoesch,[4] C. Berthod,[5] and C. Monney[1]
[1]*Department of Physics and Fribourg Center for Nanomaterials, University of Fribourg, Chemin du Musée 3, 1700 Fribourg, Switzerland*
[2]*Hiroshima Synchrotron Radiation Centre, Hiroshima University, 2-313 Kagamiyama, Higashi-Hiroshima 739-0046, Japan*
[3]*École Polytechnique Fédérale de Lausanne (EPFL), 1015 Lausanne, Switzerland*
[4]*Deutsches Elektronen-Synchrotron, Notkestrasse 85, 22607 Hamburg, Germany*
[5]*Department of Quantum Matter Physics, University of Geneva, 24 quai Ernest-Ansermet, 1211 Geneva, Switzerland*

(Received 1 November 2019; published 13 January 2020)

We revisit charge density wave (CDW) behavior in the archetypal quasi-one-dimensional (quasi-1D) material $NbSe_3$ by high-resolution angle-resolved photoemission spectroscopy measurements utilizing a microfocused laser with a photon energy of 6.3 eV. We present a detailed view of the electronic structure of this complex multiband system and unambiguously resolve CDW gaps at the Fermi level (E_F). By employing a tight-binding model, we argue that these gaps are the result of interband coupling between electronic states that reside predominantly on distinct 1D chains within the material. Two such localized states are found to couple to an electronic state that extends across multiple 1D chains, highlighting the importance of a higher-dimensional interaction in stabilizing the CDW ordering in this material. In addition, the temperature evolution of intrachain gaps caused by the CDW periodicities far below E_F deviate from the behavior expected for a Peierls-type mechanism driven by nesting; the upper and lower bands of the renormalized CDW dispersions maintain a fixed peak-to-peak distance while the gaps are gradually removed at higher temperatures. This points toward a gradual loss of long-range phase coherence as the dominant effect in reducing the CDW order parameter, which may correspond to the loss of coherence between the coupled chains. Furthermore, one of the gaps is observed above the bulk and surface CDW transition temperatures, implying the persistence of short-range incoherent CDW order. The influence of such higher-dimensional interactions likely plays an important role in a range of low-dimensional systems.

DOI: 10.1103/PhysRevB.101.045412

I. INTRODUCTION

Investigating the emergence of ordered phases such as superconductivity, magnetism, and charge density waves (CDWs) is fundamental to furthering our understanding of microscopic interactions in condensed matter. In particular, it is hoped that studying competing or coexisting orders will allow the elucidation of the roles played by different degrees of freedom in driving such exotic phenomena. Prominent examples are charge ordering [1–5] and short-range charge or magnetic order [6–8] close to superconductivity. An intriguing piece of the puzzle is that many materials exhibiting ordered phenomena are electronically low dimensional, whereby the electronic wave functions are strongly confined to exist in a plane [two dimensional (2D)] or within a chain [one dimensional (1D)]. In such reduced-dimensional systems, a relevant question is to what extent the coupling to a higher-dimensional environment affects their inherent interactions and the emergence of ordered phenomena [9]. Recent results have shown the importance of interplane Coulomb coupling for charge degrees of freedom in an otherwise 2D material [10]. Dimensional considerations have also been highlighted in 2D transition metal dichalcogenides (TMD), for example in the CDW mechanisms of $NbSe_2$ [11–13] and $TiSe_2$ [14], as well as in the superconducting mechanism of TaS_2 [15]. Given the ongoing interest in producing TMD heterostructures [16–18], as well as the possibility of probing quasi-1D effects in TMDs and other materials [19–22], the relevance of mixed dimensionality systems with weak coupling between chains or layers is clear. Here, we focus on $NbSe_3$, a paradigmatic quasi-1D CDW material, in order to reveal the influence of higher-dimensional interactions on charge ordering within a low-dimensional system.

$NbSe_3$ undergoes CDW transitions at $T_1 = 145$ K and $T_2 = 59$ K [23] with incommensurate modulation wave vectors $\boldsymbol{q}_1 = (0, 0.243, 0)$ and $\boldsymbol{q}_2 = (0.5, 0.263, 0.5)$, respectively, in units of the reciprocal lattice parameters (a^*, b^*, c^*) [24,25] as drawn in Fig. 1(b). The unit cell of $NbSe_3$ contains three pairs of inequivalent triangular prism chains, characterized by the Se-Se bond length which forms the base of the triangle in the *ac* plane [see Fig. 1(a)]. The real-space extent of the CDW vectors can be seen in Ref. [26]. Nuclear magnetic resonance [27,28] and x-ray diffraction [29] measurements have found that the $\boldsymbol{q}_1$ CDW predominantly resides on the Nb atoms of type III chains, while the $\boldsymbol{q}_2$ CDW exists mainly on chains of type I. This was supported by scanning tunneling microscopy (STM) measurements, with the additional

*christopher.nicholson@unifr.ch

 ©2020 American Physical Society

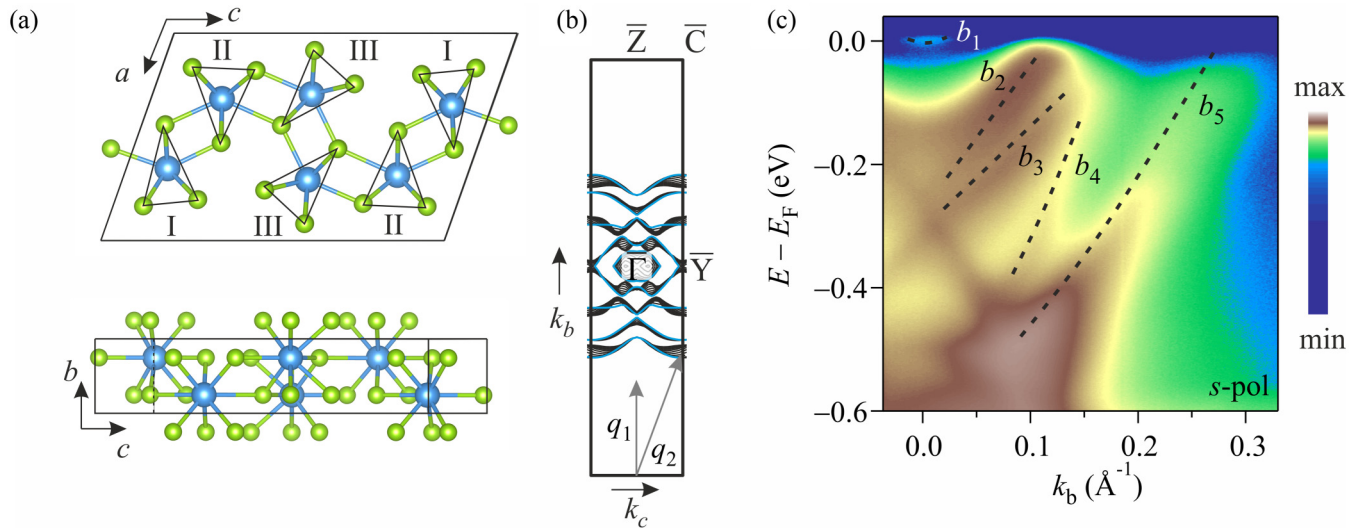

FIG. 1. (a) Atomic structure of $NbSe_3$ in the *ac* plane (upper) and *bc* plane (lower). The different chains are emphasized by the marked triangles and are numbered according to the Se-Se distances at the base of the triangle, i.e., chain I: 2.49 Å; chain II: 2.91 Å; chain III: 2.37 Å [24]. Weaker bonds between chains are also shown. (b) DFT calculated Fermi surface and surface Brillouin zone. The $k_z = 0$ cuts are highlighted in blue. The magnitude of the q_1 and q_2 wave vectors in the *bc* plane are represented as gray arrows. (c) Overview of ARPES data acquired close to the $\overline{\Gamma}$-$\overline{Z}$ plane with *s*-polarized light showing the five expected bands centered at $\overline{\Gamma}$. Data are presented on a log color scale; dashed lines are a guide to the eye.

observations of a weak contribution of the $\boldsymbol{q}_1$ CDW on chain II and unexpectedly strong contribution of $\boldsymbol{q}_2$ CDW on chain III [26]. In addition, x-ray diffraction has suggested the possibility of an interaction between the different chains [29]. In fact, it has been proposed that the interchain Coulomb coupling may even facilitate CDW formation [30,31]. These results raise questions regarding the strength of the interactions between these chains, and significance of such interactions in CDW formation.

Early angle-resolved photoemission spectroscopy (ARPES) measurements suggested a Peierls mechanism for the CDWs resulting in a gap opening at E_F due to nesting between different bands at specific points on the quasi-1D Fermi surface [32,33]. However, an unambiguous confirmation of CDW gaps at the Fermi level has proved challenging [34,35], in part due to the difficulty of separating multiple overlapping bands near E_F, and the power-law-like depletion of spectral weight observed in this system [34] which obscures the low-energy dispersions. Recent ARPES work suggested the existence of a novel 1D order [35] implying an origin of the CDWs beyond Fermi-surface nesting. In fact, a number of observations seem at odds with a typical Peierls nesting scenario, including the lack of a Kohn anomaly [36], a non-mean-field temperature dependence of the q_1 gap [37], and the power-law dependence of spectral weight close to E_F [34]. Indeed, despite the clear real-space anisotropy inherent to $NbSe_3$ single crystals, which grow as micrometer-sized hairlike needles, x-ray diffraction [24,38], scanning tunneling microscopy (STM) [39], and ARPES [34] have all shown that $NbSe_3$ develops higher-dimensional coherence at low temperatures, indicating that a simple 1D description does not suffice to explain the observed CDW behavior. This suggests that Fermi-surface nesting is not sufficient to explain CDW formation in $NbSe_3$. One possible alternative is a strong coupling between the electronic and lattice subsystems as discussed in relation to other quasi-1D systems [40], that could result in a charge transfer between chains and a change in the bonding conditions as a function of temperature [41]. This demands further investigation with ultra-high-energy resolution, high-statistics ARPES measurements in the region near E_F, with a spot size small enough to probe the small crystals of this material.

In this paper, we employ microfocus laser ARPES at 6.3 eV with a total energy broadening of less than 2.5 meV and a microfocused spot of less than 5 μm in order to determine in detail the electronic structure of $NbSe_3$ close to E_F. We demonstrate the existence of gaps at E_F related to CDW formation, and confirm the existence of gaps caused by the same CDWs at lower energies as observed previously [34]. A tight-binding simulation of the electronic structure shows that the gaps at E_F result from interband coupling, in contrast to the gaps at lower energies which are caused by intraband coupling. DFT calculations reveal that most bands have electronic density localized on separated chains in the real-space unit cell. However, one particular state has electronic density on multiple chains, and coupling to more localized states results in the CDW gaps. This clearly supports a more three-dimensional (3D) nature of the electronic wave functions at low temperatures, and provides a microscopic picture of the CDW. In addition, we find that with increasing temperature the magnitude of the gaps caused by the CDW at lower energies remain constant, in contrast to the expectations for a Peierls system. The upper and lower renormalized CDW bands gradually broaden and merge, which points to a gradual loss of long-range phase coherence as the mechanism removing the order parameter. The fact that the dimensionality of charge excitations is known to change in this material as a function of temperature [24,34,38,39] further hints that the relevant coherence may be between the different chains,

highlighting the importance of the role played by higher-dimensional interactions in stabilizing the charge order.

II. METHODS

Clean surfaces of $NbSe_3$ single crystals with typical dimensions $20 \times 500\ \mu m^2$ were prepared by scotch tape cleaving in ultrahigh vacuum better than 2×10^{-10} torr at room temperature. ARPES measurements were carried out using the μ-laser ARPES system at the Hiroshima Synchrotron Radiation Centre (HiSOR) [42] over a temperature range 26–180 K. Photons with energy 6.3 eV (197 nm) were generated using a mode-locked Ti:sapphire laser at 80-MHz repetition rate with 10-ps pulse duration to drive frequency addition in nonlinear optical crystals. An angular resolution better than 0.05° and total energy broadening less than 2.5 meV were used. The light polarization was set to p and s configurations via a zero-order $\lambda/2$ wave plate. The laser was focused on to the sample with a spot size of less than 5 μm, which is sufficiently small to resolve individual single-crystalline domains. The work function of the sample was measured to be 5.0 eV.

A tight-binding model was constructed to aid the interpretation of the low-energy electronic structure. The model focuses on the key ingredients required in order to reproduce qualitatively the experimental intraband and interband CDW gaps. We adopted a two-dimensional, three-orbital model for the bands b_2, b_3, and b_5, parametrized by orbital-dependent onsite energies and nearest-neighbor hopping amplitudes along the b and c axes. The Hamiltonian for the CDW was built by considering two cosine potentials with wave vectors q_1 and q_2 along the b axis and studying the matrix elements in the basis of Wannier functions. For slowly varying potentials, the leading matrix elements are diagonal in the band index and open the intraband gaps, while subsequent terms are dipolar and mostly off diagonal (they involve the gradient of the CDW potential) and open the interband gaps. While the diagonal terms were considered in our previous work [34], the off-diagonal ones were not previously considered as our previous data did not resolve the relevant bands near E_F. Here, we set them using three parameters x_{23}, x_{25}, and x_{35} having the unit of a length. Full details of the model and all its parameters are given in Appendix B.

In Appendix B, the matrix elements of the CDW potential are discussed using the Wannier functions as a basis. These functions are well defined in principle but difficult to determine in practice in $NbSe_3$, due to the intricate entanglement of bands. In order to visualize the localization of the charge associated with each band, we consider instead the quantity $\sum_{\boldsymbol{k}} |u_{\boldsymbol{k}n}(\boldsymbol{r})|^2$, where $u_{\boldsymbol{k}n}(\boldsymbol{r})$ is the periodic part of the Bloch function for band n. If the bands could be disentangled and the $\boldsymbol{k}$ sum were extended across the entire Brillouin zone, $\sum_{\boldsymbol{k}} |u_{\boldsymbol{k}n}(\boldsymbol{r})|^2 = \sum_{\boldsymbol{R}} |w_{\boldsymbol{R}n}(\boldsymbol{r})|^2$ would be a periodic function of $\boldsymbol{r}$ obtained by superimposing the probability densities of the Wannier states $w_{\boldsymbol{R}n}(\boldsymbol{r})$ from all unit cells of the Bravais lattice defined by the vectors $\boldsymbol{R}$. By restricting the $\boldsymbol{k}$ sum to the Fermi surface of band n, we focus on the states at the Fermi level which are affected the most by the CDW. The quantity $\sum_{\boldsymbol{k}} |u_{\boldsymbol{k}n}(\boldsymbol{r})|^2 \delta(E_{\boldsymbol{k}n})$ is nothing other than the band-resolved local density of states at the Fermi level and gives information about the spatial localization of states at the Fermi level.

We have performed this calculation using the OPENMX density functional theory (DFT) code [43–46] which uses norm-conserving pseudopotentials and pseudoatomic localized basis functions. The ground-state calculation used the PBE-GGA functional [47] and the atomic basis sets for Se and Nb were set as Nb7.0-$s^3p^3d^2f^1$ and Se7.0-$s^3p^3d^3f^1$, respectively. This choice of basis has been shown to reproduce elastic and electronic properties of elemental Se and Nb that are well comparable to WIEN2K [48] calculations with (RMT $\times$ KMAX $=$ 12). The energy cutoff was 350 Ry and the Brillouin zone was sampled with a $6 \times 24 \times 4$ grid. Both lattice constants and fractional atomic coordinates were set to the experimental values of the non-CDW unit cell [24]. The functions $u_{\boldsymbol{k}n}$ were calculated across the Fermi surface at various points in the (k_b, k_c) plane for each of the b_n bands ($n = 1$–5). Along k_b steps of 0.001 of the Γ-Γ distance were chosen and the k_c direction was sampled with steps of 0.01 times the Γ-Γ distance along k_b. We have confirmed that the addition of further $\boldsymbol{k}$ points does not significantly alter the calculated outcome. In order to restrict the calculation to the region of the Fermi surface, the contribution of each occupied state was given a Gaussian weight $\exp[-(E_B/7.5\ \text{meV})^2]$ and states with binding energy E_B larger than 20 meV were ignored.

III. RESULTS AND DISCUSSION

A. Low-energy electronic structure

ARPES measurements obtained with the μ-focus laser in the $\overline{\Gamma}$-$\overline{Z}$ plane close to $\overline{\Gamma}$ in the $\overline{\Gamma}$-$\overline{Y}$ direction of the surface Brillouin zone are presented in Fig. 1(c). This reveals the five bands predicted by DFT [32] and resolved previously by ARPES [34]. The data are presented on a logarithmic color scale due to the high intensity of the band b_5 at lower energies compared with states close to E_F. The separation of bands and their individual dispersions in the raw data are considerably clearer compared with our previous study, particularly in the region of bands b_2 and b_3. The observation of the small b_1 pocket is consistent with the STM measurements of Ref. [26], which explained the observed bias-voltage dependence by postulating a b_1 band with a very shallow minimum below E_F.

To obtain a more detailed view on the electronic states, we focus on the two regions presented in Figs. 2(a) and 2(c), which highlight the dispersions of bands b_2/b_3 and band b_5, respectively. Fitting of the energy distribution curves (EDCs) with Gaussians allows the extraction of the band dispersions. Representative results are shown in Figs. 2(b) and 2(d). In the case of bands b_2 and b_3, maxima are reached at 0.125 and 0.135 Å^{-1}, respectively, after which the bands turn toward higher binding energy, leaving gaps of 50 and 95 meV ($\pm$5 meV) between the band maximum and E_F. We note that a similar backfolded dispersion can be discerned in band b_2 in Fig. 1(c), although less clearly due to the log color scale. Unambiguously observing CDW gaps at E_F in $NbSe_3$ has proved challenging due to the multiple overlapping bands and the necessity of very small spot sizes to measure the tiny needlelike crystals. Previous studies that found evidence of gaps at E_F were unable to fully disentangle the dispersions of bands b_2 and b_3 [32–34], thereby making a precise

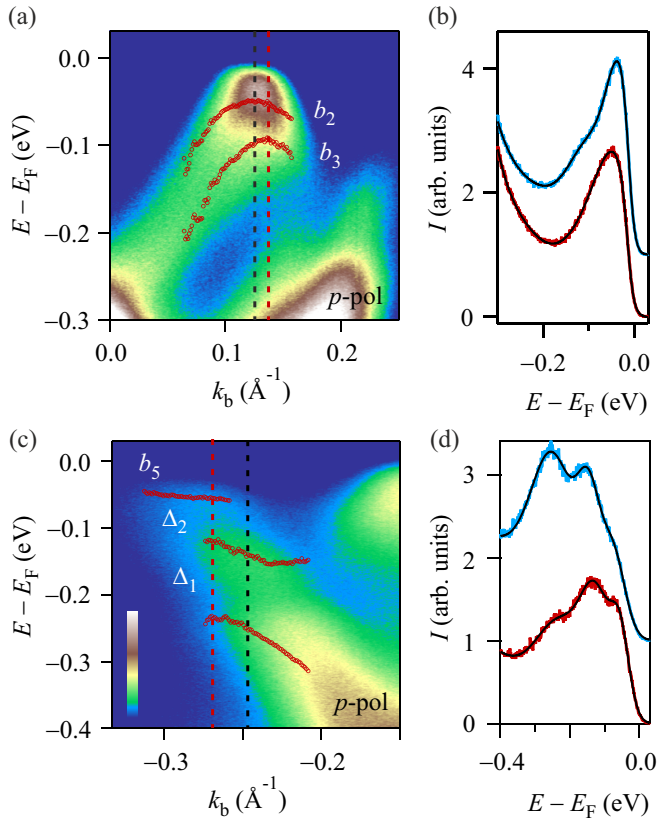

FIG. 2. (a) Zoom on bands b_2 and b_3 close to E_F with p-polarized light (linear color scale). EDC fitting results are overlaid to highlight the dispersion. (b) Individual EDCs taken at the k position of the band apexes [0.12 Å^{-1} (blue) and 0.14 Å^{-1} (red)] revealing the CDW gaps. (c) Zoom on band b_5 at higher momenta with p-polarized light showing the gaps previously observed in [34]. (d) Individual EDCs taken at −0.25 Å^{-1} (blue) and −0.27 Å^{-1} (red) highlighting the peaks of the renormalized dispersions. All data acquired at 26 K.

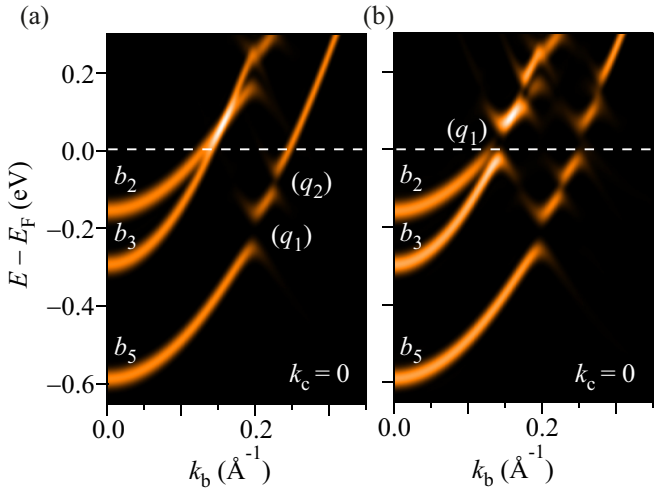

FIG. 3. Simulated spectral function including CDW periodicities within the tight-binding model described in the text including (a) only intraband coupling and (b) both intraband and interband couplings. This reveals the gaps at E_F in bands b_2 and b_3 are caused by the respective interband coupling of bands b_2 and b_3 with b_5. The gaps in band b_5 are confirmed as resulting from intraband coupling due to the backfolded bands caused by the q_1 and q_2 periodicities. The wave vectors of the CDWs responsible for opening the gaps discussed in the text are labeled in brackets. Plots with all bare and backfolded dispersions overlaid are shown in Fig. 9.

determination of the gap size difficult. Nevertheless, our current determination of the gap size is in good agreement with both previous STM [49] and ARPES measurements [33,34]. The dispersion in band b_5 [Fig. 2(c)] confirms the previous observations of gaps resulting from the CDW periodicities below E_F at around −0.2 eV [32–34] and −0.1 eV [34] ascribed to the backfolding of band b_5 onto itself by q_1 and q_2, respectively. We note the similarity in dispersions obtained with s-polarized light in Fig. 1(c) compared with p-polarized light in Figs. 2(a) and 2(c), in contrast to the data of Ref. [35] where polarization-dependent matrix elements were proposed to explain the observed differences between s- and p-polarized light. This discrepancy may be due to the photoemission final states being less well defined in the current experiments due to the low photon energy used. Compared with the results obtained in Ref. [35] at higher photon energies, this may lead to a reduction of the dichroic signal in this system.

B. Tight-binding model and DFT

To determine the origin of the CDW gaps in bands b_2, b_3, and b_5, we use a tight-binding model, the results of which are presented in Fig. 3; full details of the model are given in Appendix B. We first consider only intraband coupling, which mixes the original bands with their own CDW replicas and allows gaps to open. Previously [34], and here in Fig. 3(a), the gaps in b_5 indeed appear at positions where the original b_5 overlaps with its replicas centered at the q_1 and q_2 wave vectors. For completeness, the tight-binding model with all bare and backfolded dispersions overlaid is shown in Appendix B, Fig. 9. Conversely, no gaps appear in either b_2 or b_3 near E_F, as overlap with their own CDW replicas occurs only well above E_F. The situation changes, however, once interband coupling is included in the model. Figure 3(b) shows the case with $x_{23} = 0$ and $x_{25} = x_{35} = b/2$, where b is the lattice constant along the chains and x_{nm} sets the matrix element between bands n and m. In this case, both bands b_2 and b_3 become gapped at E_F as a result of the overlap between their original dispersions and the b_5 band backfolded by q_1. This extends the description given in Ref. [33]. For both b_2 and b_3 the replica of b_5 backfolded by q_2 only opens gaps above E_F. The model therefore allows us to distinguish between the effects of intraband and interband coupling and their respective role in the low-temperature electronic structure.

The formation of CDW gaps at E_F via interband coupling raises the question of how much the electronic densities corresponding to the various bands overlap in real space. To address this we have used DFT to calculate the electronic density distributions of states near the Fermi level associated to bands b_{1-5}, as described in Sec. II. The results are plotted on top of the atomic structure in Figs. 4(a)–4(c). Band b_3 is found to be the most strongly localized in real space, essentially being completely confined to type III chains. Band b_2 on the other hand does not appear at all on type III chains

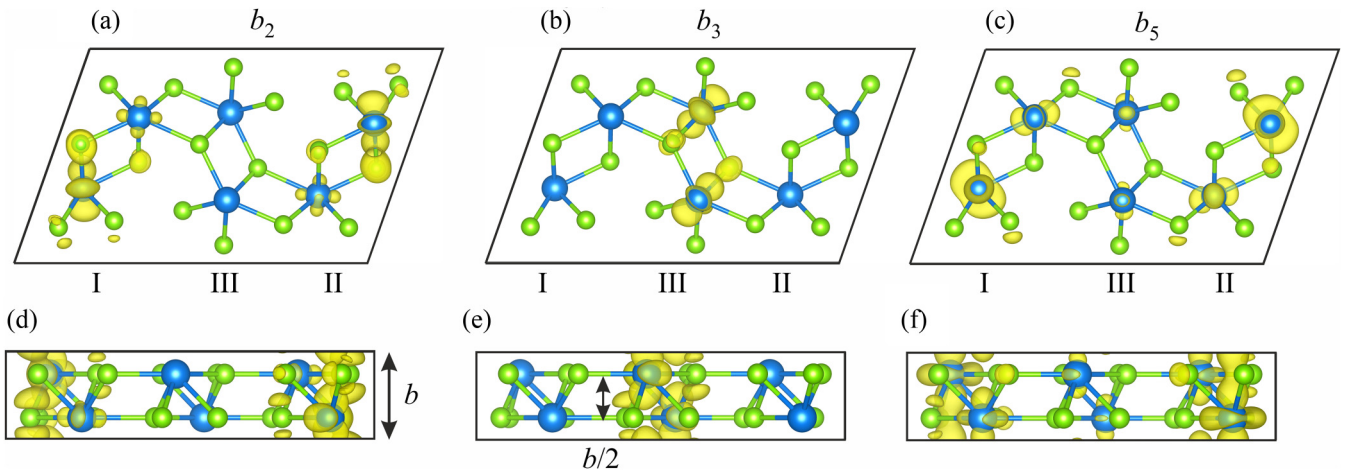

FIG. 4. (a)–(c) DFT calculated spatial distribution of electronic density in the *ac* plane corresponding to states near the Fermi surface in bands b_2, b_3, and b_5. (d)–(f) The same calculated distributions shown in the *bc* plane. All isosurfaces are plotted at the same value of electron density. From these plots it can be seen that bands b_2 and b_3 have negligible spatial overlap, whereas both overlap with b_5, which is found on all three chain types. This overlap allows the coupling that leads to the interband gap opening. The values of the coupling parameters $x_{25} = x_{35} = b/2$ mean that, on average, the distance between the probability densities of the corresponding orbitals along the b axis is $b/2$.

at this level of density visualization, and instead has strong amplitude on chains of types I and II. This means that bands b_2 and b_3 have negligible spatial overlap and therefore will not couple. Importantly, band b_5 is found to have distinct contributions across all three chain types and can therefore mediate interband coupling across the three different chains, allowing for the hybridizationlike gaps in b_2 and b_3 to open at E_F (for a full description, see Appendix B). Such an interchain mixing of states highlights the higher-dimensional nature of the CDW phase in $NbSe_3$ at low temperatures, as previously suggested by multiple techniques, and may also explain the observation with STM of strong contributions of different CDW q vectors occurring on different chain types [26].

C. Temperature dependence of gaps

In the classic Peierls picture, both the electronic gap opening at E_F due to the lattice distortion and the long-range phase coherence of this order develop at the transition temperature. Upon lowering the temperature further, the electronic gap gradually widens at the same time as the atomic displacement increases. Such expectations hold in the limit of weak electron-phonon coupling, but in materials with a strong or k-dependent coupling there is the possibility that the electronic gap survives above the transition temperature and short-range distortions of the CDW persist [50]. The observation of a gap above T_c in ARPES has previously been reported in various materials [51–54].

To investigate the possibility of such behavior in $NbSe_3$ we have performed temperature-dependent measurements over the range 26–180 K, which encompasses both CDW transition temperatures. We have focused mainly on the evolution of the CDW gaps in band b_5, as in the region of E_F where gaps occur in bands b_2 and b_3 the spectral weight develops a power-law-like dependence at higher temperatures [Fig. 6(a)], which complicates the analysis of the gap. Nevertheless, the intensity close to E_F will also be discussed briefly below. The EDCs presented in Figs. 5(a) and 5(b) are obtained at the two positions marked by dashed lines in Fig. 2(c). The two peaks correspond to the upper and lower parts of the renormalized dispersions, respectively, and therefore reveal the gap sizes. A third peak can be seen in each panel since the EDCs at each position overlap a little with the neighboring gap. Upon increasing the temperature, the gaps are gradually removed.

In order to obtain the evolution of the gap size as a function of temperature, we have fitted the EDCs with three Gaussians [overlaid in Figs. 5(a) and 5(b)] to extract the peak positions and corresponding gap sizes, which are presented in Fig. 5(c). Within error bars the gap size is constant over the full temperature range in both cases [Fig. 5(c)], i.e., the distance between peaks does not change. Additionally, the two peaks of the Δ_2 gap persist to at least 84 K, above the bulk transition temperature of the q_2 CDW 59 K and even above the surface transition temperature of 75 K obtained with STM [39]. Evidence of short-range CDW order has also been found in x-ray scattering data around 10 K above the q_1 [38] and q_2 transitions [31].

We note that fitting at higher temperatures becomes much less well defined due to the broadening of the EDCs. In the region of the gap, this is likely a result of a mixture of effects: broadening due to increased electron-phonon scattering at higher temperatures and the intrinsic removal of the gap. Distinguishing these effects is a delicate matter, and is beyond the scope of this paper. However, the fact that multiple effects may contribute simultaneously does not change the central result: that the relative positions of the upper and lower CDW dispersions, and therefore the CDW gaps, do not change as a function of temperature. Since it is known that the CDWs do not survive up to room temperature, a mechanism is still required to remove the gaps. Our data are therefore suggestive of a loss of phase coherence as the mechanism by which the CDW is removed, rather than it closing in a Peierls-type manner. This hypothesis is supported by temperature-dependent x-ray diffraction measurements (see Appendix A, Fig. 8) which find an increase of intensity in the CDW superstructure peaks, implying increased coherence length at low temperatures.

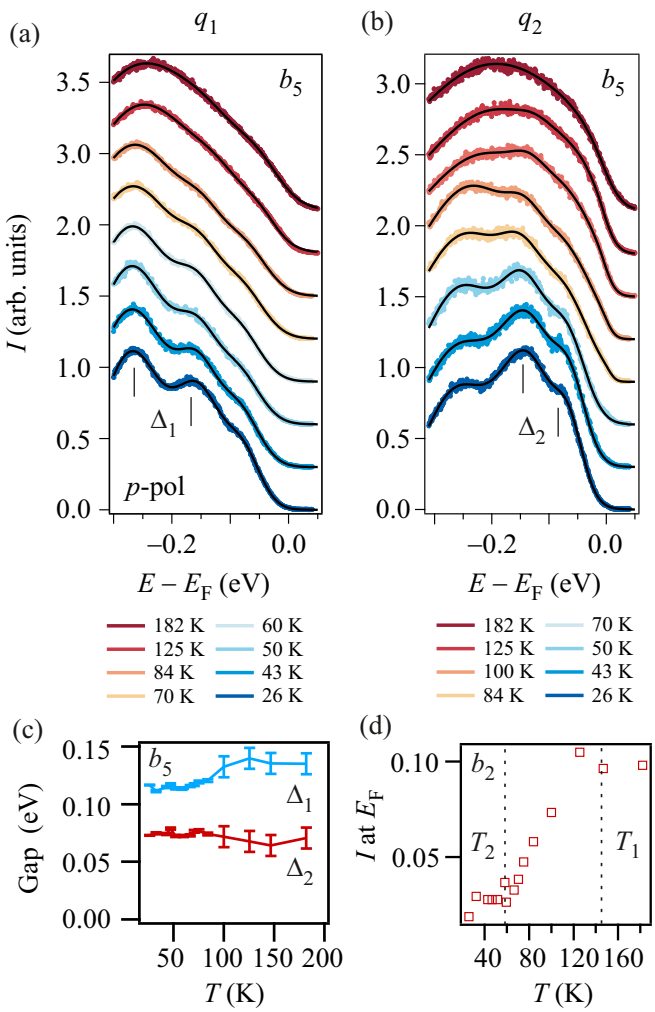

FIG. 5. Temperature dependence of EDCs at k points corresponding to the CDW gap positions in band b_5. The EDCs in (a) at $k_b = -0.25$ Å^{-1} correspond to the lower-energy gap and (b) at $k_b = -0.27$ Å^{-1} to the upper. Curves are offset vertically for clarity. The Δ_2 gap can be seen in the EDCs until at least 84 K, which is above the expected surface transition temperature. (c) Gap size of q_1 and q_2 CDWs in band b_5 extracted through fitting of temperature-dependent EDCs. The gap size is found to remain constant within error bars as the temperature is increased but the gap is gradually removed at higher temperatures, pointing toward a loss of phase coherence as the mechanism removing the CDW. (d) Intensity of band b_2 at E_F revealing clear changes in the spectral weight at E_F between the two transition temperatures.

Curiously, the band positions themselves are not constant, even though the gaps sizes are. This is evidenced by a shift of both upper and lower dispersions by around 30 meV as a function of temperature [Figs. 7(a) and 7(b)]. A similar shift is observed in band b_3 well away from E_F. This rigid band shift of multiple bands is suggestive of a change in the chemical potential as a result of the CDW gap opening, but may also result from the transfer of charge between Nb atoms on different chains [41]. The exact relation of this shift to CDW formation is unclear at present. This slight shift of the bands may also be partially reflected in the change of spectral weight at E_F [Fig. 5(d)]. Here, one sees the increase

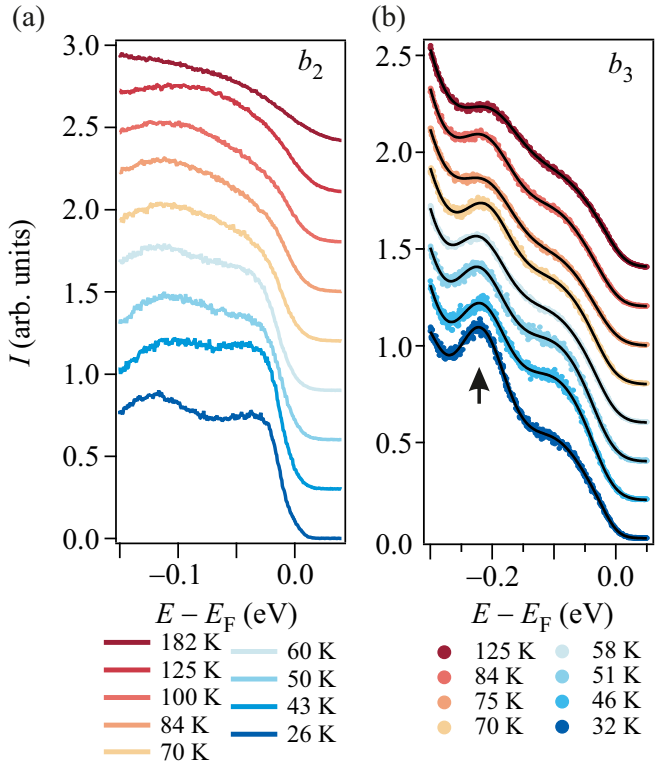

FIG. 6. (a) Temperature-dependent EDCs obtained at $k = 0.135$ Å^{-1} revealing the evolution of the CDW gap at E_F into the power-law line shape characteristic of the high-temperature phase. (b) Temperature-dependent EDCs of band b_3 at $k_b = 0.06$ Å^{-1} which are fitted to extract the rigid band shift shown in Fig. 7(c).

of spectral weight with increasing temperature, again over the temperature region defined by the two CDW transitions. However, given the change in line shape at higher temperatures which becomes power-law like, it is difficult to say exactly what mechanism causes the change of spectral weight and what relation this bears to the macroscopic properties of this material.

D. Discussion

The present observations of CDW gaps with interchain character highlight the role that higher-dimensional interactions play in stabilizing the long-range CDW order in $NbSe_3$. In addition, the fact that the CDW appears to be removed via a loss of phase coherence, as evidenced by the gradual removal of the CDW gaps at constant gap size suggests the CDW ordering is influenced by the phase coherence between chains. This leads us to the following picture of how the CDW is removed: At low temperatures, CDW order is well developed and is stabilized by long-range coherent electronic states across the chains in a 3D environment. As the temperature is increased, the coherence of the electronic states reduces, with the result that they become more localized to individual chains, thereby gradually reducing the dimensionality of the system and weakening the interchain CDW phase coherence. At higher temperatures, the CDW is completely washed out as the electronic states become localized to individual chains due to their very short coherence lengths and therefore the

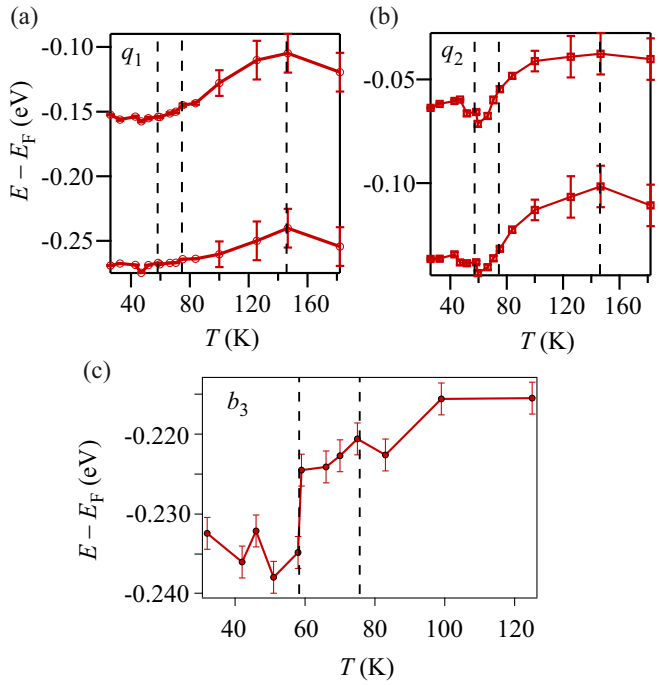

FIG. 7. Intraband gap edges extracted from fitted peak maxima as a function of temperature in band b_5 for (a) the q_1 and (b) the q_2 CDWs. All bands are found to shift over a temperature range between the two CDW transitions. T_2, $T_{2,\text{surface}}$, and T_1 are marked by dashed lines from left to right. The corresponding raw data and extracted gap sizes are shown in Fig. 5. (c) Extracted position of band b_3 from the EDCs in Fig. 6 marked by the arrow.

interchain phase coherence is lost. The high-temperature 1D phase may also host exotic behavior such as the Tomonaga-Luttinger liquid. Such a picture complements the description given in our previous publication where we estimated the effective crossover energy scale from 3D to 1D based on a tight-binding fit of the quasi-1D Fermi surface [34]. This

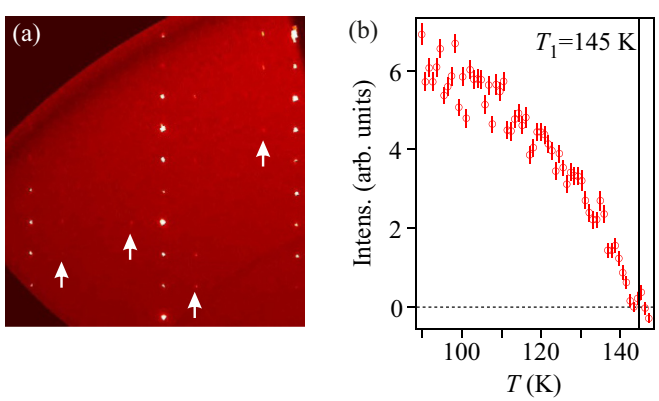

FIG. 8. (a) X-ray diffraction intensity in the reconstructed (5 kl) plane at 80 K. Superstructure spots corresponding to the q_1 CDW are marked by the white arrows. (b) Intensity of the (1, 1.241, 0) spot, corresponding to the q_1 CDW, as a function of temperature. Intensity above the background (subtracted) for this peak first appears at $T_1 = 145$ K. The gradual increase of the peak intensity implies the increase of the CDW correlation length toward lower temperatures.

revealed 3D behavior at low temperatures is in accordance with a number of previous works [24,38,39] which can be seen in light of the above discussion as resulting from the increase of electronic coherence between chains.

That the CDW order parameter is removed by phase incoherence, rather than amplitude reduction, itself implies a mechanism different to the traditional Peierls model. An alternative description such as the metal-metal bonding approach proposed by Wilson [41] may be appropriate, which is analogous to the Jahn-Teller distortion in molecules. In this scenario, a change of orbital occupancy as a function of temperature modifies the bonding and antibonding populations for particular bonds, stabilizing the CDW. Similar conclusions were drawn from the calculations of Ref. [30] which further highlighted the role of interchain Coulomb interactions in stabilizing the CDWs in $NbSe_3$. The observation of the rigid band shift during CDW formation presented above may indeed point in the direction of a redistribution of charge in the Nb states at E_F, although the details remain unclear. The potential relevance of such a description can also be seen in the context of recent time-resolved experiments on femtosecond timescales where the transient occupation of bonding and antibonding states was shown to photoinduce a CDW transition [55] in another quasi-1D system. The band shift and gradual gapping of the Fermi surface as seen in Figs. 7 and 5(d) therefore suggest a more chemical-like description of the CDW. On the other hand, the shift of the bands may be explained by a shift of the chemical potential due to the opening of the CDW gaps at E_F. An analysis of this is therefore complicated by the power-law depletion that obscures the gap at E_F. Further studies in this direction may shed light on the role of particular state occupancies on the CDWs.

Further evidence of a non-Peierls scenario comes from the distribution of spectral weight close to E_F, which has the form of a power law or pseudogap at low temperatures [34]. Such behavior has been observed in a number of quasi-1D systems, although to date no general explanation has been found for this. Some instances have been attributed to Tomonaga-Luttinger-liquid (TLL) behavior [56–59], where all spectral functions are predicted to take a power-law form [60,61], although other signatures of TLL behavior in these materials such as spin-charge separation have proved elusive. As discussed above, we predict that TLL behavior should only appear at higher temperatures in $NbSe_3$ once the phase coherence of electronic states is reduced, restricting them to individual chains.

We note finally that strong-coupling theory predicts CDW distortions commensurate with the lattice periodicity, while the weak-coupling limit tends to favor incommensurate distortions. It is interesting to consider, therefore, that the combined CDWs in $NbSe_3$ are "nearly commensurate," meaning that the combined period of the $q_1 + q_2$ is close to an integer number of lattice constants. This hints at an intermediate-coupling strength in $NbSe_3$. The current observations in $NbSe_3$ therefore suggest the appropriateness of a description where the role of Fermi-surface nesting is marginalized, and where k-dependent electron-phonon interaction as well as interchain coupling play central roles [30].

IV. SUMMARY

We have investigated the electronic structure of $NbSe_3$ in the vicinity of E_F using μ-spot laser ARPES with very-high-energy resolution. We have clearly demonstrated gaps due to CDW formation both at and below E_F. We have discussed their origin in terms of interband and intraband matrix elements, respectively, and placed this in the context of the spatial extent of the related electronic densities, which are predominantly found to reside on individual 1D chains, but with coupling mediated by one particular delocalized state. This highlights the higher-dimensional interactions that stabilize CDW behavior in this quasi-1D material. In addition, we have followed the renormalized dispersions as a function of temperature and found that the gap sizes stay constant, with one gap even visible above the CDW transition temperature. Since the gaps are gradually removed by broadening, we conclude that it is the loss of long-range phase coherence rather than the reduction of the CDW amplitude that removes the order parameter. It is plausible that the loss of coherence relates to the phase coherence between the electronic states on different chains that contribute to the CDW gaps. These considerations extend to other low-dimensional systems such as heterostructures of 2D TMDs or 1D edge states, where mixed dimensionality states are a topic of high current interest.

ACKNOWLEDGMENTS

The laser ARPES measurements at HiSOR were performed with the approval of the Proposal Assessing Committee (Proposal No. 16BU011). Liquid helium for the ARPES measurements was supplied by the N-BARD, Hiroshima University. We thank A. Bosak, D. Chernyshov, and P. Pattison for suggesting the x-ray diffraction data acquisitions shown in Appendix A and for help with this experiment. This project was supported by the Swiss National Science Foundation (SNSF) Grant No. P00P2_170597.

APPENDIX A: EXTENDED DATA

To show the increasing influence of the power-law spectral shape on the CDW gap at E_F as a function of temperature, Fig. 6(a) shows the EDCs through the maxima of bands b_2 and b_3. This complicates the analysis of the spectral weight and the CDW gap. Figure 6(b) shows EDCs from band b_3 from which the band shift discussed in the main text (and below) is extracted by fitting.

Although the gap sizes ($\Delta_{1,2}$) remain approximately constant as a function of temperature, as shown in Fig. 5(c) the upper and lower gap edges clearly change. In Figs. 7(a) and 7(b) the extracted positions for q_1 and q_2 related dispersions are shown, respectively. It is notable that the shift occurs exactly within the temperature region where the CDW transitions occur. A shift of the same magnitude occurring in band b_3 [Fig. 7(c)] is suggestive of a charge redistribution as discussed in the main text.

Single-crystal x-ray diffraction data were obtained at the Swiss-Norwegian beamline BL01A at the ESRF. The sample was illuminated with monochromatic x rays of 0.717-Å wavelength and stepwise rotated with 1° oscillations while acquiring the scattered x rays on an area detector (MAR345 image plate). The samples were cooled in the dry nitrogen gas flow of a cryostream cooler (Oxford Instruments). The indices of diffraction spots were determined and arbitrary planes of x-ray scattering intensity were reconstructed using the software CRYSALIS [see Fig. 7(a) for a high-symmetry plane]. The intensity of individual diffraction spots was determined against the background of adjacent diffuse x-ray scattering and background using CRYSALIS [Fig. 8(b)].

The onset of detectable intensity at the incommensurate scattering vector (1, 1.241, 0) [Fig. 8(b)] is consistent with a periodic lattice distortion (PLD) related to the CDW modulation q_1, which sets in sharply at T_1 and develops fully toward lower temperatures. This crystallographic behavior of the long-range-ordered PLD is consistent with our present ARPES observation of fixed CDW gap sizes and changes in broadening as a function of temperature.

APPENDIX B: THREE-BAND TIGHT-BINDING MODEL

A model for the effect of the CDW on the low-energy dispersion in $NbSe_3$ is most conveniently formulated in the basis of Wannier states $|\boldsymbol{R}n\rangle = N^{-1/2}\sum_{\boldsymbol{k}} e^{-i\boldsymbol{k}\cdot\boldsymbol{R}}|\boldsymbol{k}n\rangle$, where $|\boldsymbol{k}n\rangle$ are the Bloch states. $\boldsymbol{R}$ represents any vector of the Bravais lattice, n is the band index, $\boldsymbol{k}$ is a wave vector in the first Brillouin zone, and the state $|\boldsymbol{R}n\rangle$ is localized around $\boldsymbol{R}+\boldsymbol{\tau}_n$ with $\boldsymbol{\tau}_n$ some vector in the primitive cell. While the entanglement of several bands renders the practical construction of Wannier functions difficult for $NbSe_3$, it is sufficient for our purposes that they are well defined formally. In the absence of CDW, the Hamiltonian H_0 is diagonal in the band index and the matrix elements $\langle\boldsymbol{R}n|H_0|\boldsymbol{R}'n\rangle$ fall off rapidly with increasing $|\boldsymbol{R}-\boldsymbol{R}'|$. Our two-dimensional tight-binding model retains the local and nearest-neighbor matrix elements in the (b,c) plane, i.e., $\langle\boldsymbol{R}n|H_0|\boldsymbol{R}n\rangle = -\mu_n$, $\langle\boldsymbol{R}n|H_0|\boldsymbol{R}'n\rangle = -t_{nb}$ if $|\boldsymbol{R}-\boldsymbol{R}'| = b$, and $\langle\boldsymbol{R}n|H_0|\boldsymbol{R}'n\rangle = -t_{nc}$ if $|\boldsymbol{R}-\boldsymbol{R}'| = c$. The corresponding electronic dispersion is $E_{\boldsymbol{k}n} = -2t_{nb}\cos(k_b b) - 2t_{nc}\cos(k_c c) - \mu_n$. Restricting to the subspace of bands b_2, b_3, and b_5, we choose the parameters such as to fulfill the following conditions extracted from the data: the hopping amplitude along c is 27 meV [34]; the minima of b_2, b_3, and b_5 are at −0.15, −0.29, and −0.58 eV; the q_1 and q_2 gaps in b_5 are at −0.2 and −0.09 eV; the crossing between b_3 and the q_1-folded b_5 is at +20 meV; the crossing between b_2 and the q_1-folded b_5 is at +35 meV. The ensuing parameters are $(\mu_2, t_{2b}, t_{2c}) = (-1.488, 0.792, 0.027)$ eV, $(\mu_3, t_{3b}, t_{3c}) = (-2.298, 1.267, 0.027)$ eV, and $(\mu_5, t_{5b}, t_{5c}) = (-1.148, 0.837, 0.027)$ eV. The resulting bare dispersions before introduction of the CDW periodicities are overlaid in Fig. 9.

The CDW acts on the electrons as a local potential $V_{\mathrm{CDW}}(\boldsymbol{r})$. The detailed shape of this potential in real space is unknown for $NbSe_3$, except for the fact that it has two components of known periodicities. The minimal ansatz keeps only the first Fourier coefficient:

$$V_{\mathrm{CDW}}(\boldsymbol{r}) = 2V_1\cos(\boldsymbol{q}_1\cdot\boldsymbol{r}+\varphi_1) + 2V_2\cos(\boldsymbol{q}_2\cdot\boldsymbol{r}+\varphi_2). \tag{B1}$$

For simplicity, we ignore the component of $\boldsymbol{q}_2$ normal to the b axis and we "rationalize" the periods to the values $q_1 b = 7\pi/16$ and $q_2 b = \pi/2$, such that V_{CDW} is commensurate with a

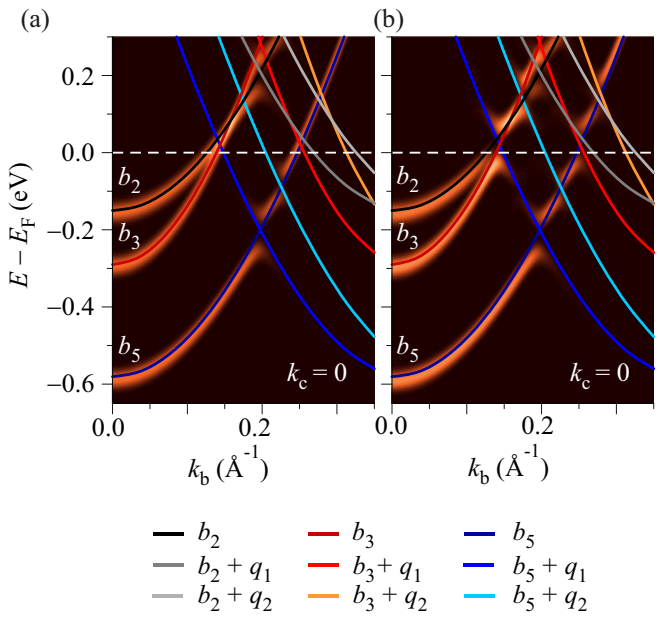

FIG. 9. Tight-binding calculations for the CDW phase as presented in the main text (a) excluding and (b) including interband coupling with the bare dispersions and those of the backfolded bands overlaid. The bare dispersion from each of the bands is labeled b_2, b_3, and b_5, respectively. The backfolded dispersions resulting from the q_1 and q_2 CDWs are color coded for clarity.

period $32b$ [34]. The amplitudes $2V_1 = 95$ meV and $2V_2 = 65$ meV are taken as the low-temperature values of the q_1 and q_2 gaps in b_5. Like for H_0, we represent V_{CDW} in the Wannier basis and retain the leading matrix elements. For evaluating the matrix element between a pair of states $|\boldsymbol{R}n\rangle$ and $|\boldsymbol{R}'m\rangle$, $V_{\mathrm{CDW}}(\boldsymbol{r})$ may be expanded around the point $\boldsymbol{r}_0 = \frac{1}{2}(\boldsymbol{R} + \boldsymbol{\tau}_n + \boldsymbol{R}' + \boldsymbol{\tau}_m)$ where the overlap of the Wannier functions is largest. The expansion is meaningful if V_{CDW} varies slowly in space in comparison to the Wannier functions. The matrix element reads as

$$\langle \boldsymbol{R}n|V_{\mathrm{CDW}}|\boldsymbol{R}'m\rangle = V_{\mathrm{CDW}}(\boldsymbol{r}_0)\langle \boldsymbol{R}n|\boldsymbol{R}'m\rangle + \nabla V_{\mathrm{CDW}}(\boldsymbol{r}_0) \cdot \langle \boldsymbol{R}n|\boldsymbol{r} - \boldsymbol{r}_0|\boldsymbol{R}'m\rangle + \cdots . \tag{B2}$$

Owing to the orthogonality of the Wannier states, the first term in the right-hand side of Eq. (B2) is diagonal and shifts the onsite energies by the orbital-dependent value $V_{\mathrm{CDW}}(\boldsymbol{R} + \boldsymbol{\tau}_n)$ without mixing the bands. The second term of the expansion has in general both diagonal and off-diagonal contributions in the band indices, that fall off rapidly with increasing $|\boldsymbol{R} - \boldsymbol{R}'|$. The terms with $|\boldsymbol{R} - \boldsymbol{R}'| = b$ change the hopping amplitudes t_{nb} by a value modulated in space according to the CDW. As $V_1, V_2 \ll t_{nb}$, we neglect these changes and retain intracell terms with $\boldsymbol{R} = \boldsymbol{R}'$. Furthermore, we ignore the diagonal terms proportional to $\langle \boldsymbol{R}n|\boldsymbol{r} - \boldsymbol{r}_0|\boldsymbol{R}n\rangle$, as these terms vanish identically for Wannier functions that have inversion symmetry around the point where they are localized. Our minimal tight-binding model for the CDW finally reads as

$$\langle \boldsymbol{R}n|V_{\mathrm{CDW}}|\boldsymbol{R}'m\rangle \approx \delta_{\boldsymbol{R}\boldsymbol{R}'}\left[\delta_{nm}V_{\mathrm{CDW}}(\boldsymbol{R} + \boldsymbol{\tau}_n) + (1-\delta_{nm})\boldsymbol{d}_{nm} \cdot \nabla V_{\mathrm{CDW}}\left(\boldsymbol{R} + \frac{\boldsymbol{\tau}_n + \boldsymbol{\tau}_m}{2}\right)\right]. \tag{B3}$$

The components of the vectors $\boldsymbol{d}_{nm} = \langle \boldsymbol{0}n|\boldsymbol{r} - (\boldsymbol{\tau}_n + \boldsymbol{\tau}_m)/2|\boldsymbol{0}m\rangle$ along b are the only ones required, as the gradient of the CDW potential lies along the b axis. This is the case since we do not include any CDW modulation along the a or c directions. We denote these components x_{23}, x_{25}, and x_{35}.

According to the above, nonzero matrix elements between bands occur via the dipole operator and are maximized for Wannier states that have sufficient overlap while being separated along the b axis. Under the, reasonable, assumption that the probability density of Wannier states is similar to the distribution of electronic density as displayed in Fig. 4, a nonzero matrix element requires electronic density that is both on the same chain and distant along b. As can be seen from Fig. 4, this condition is met for both the b_2-b_5 and b_3-b_5 states, but not for b_2-b_3 due to the spatial separation of these states in the (a, c) plane. This therefore justifies the choice of the x_{nm}'s in the tight-binding model ($x_{23} = 0, x_{25} = b/2, x_{35} = b/2$).

We compute the spectral function using a Chebyshev expansion as explained in Ref. [34]. The order of this expansion is such that the energy resolution is 40 meV, which leads to a broadening of the bands as seen in Fig. 3. Our calculations show that the spectral function is insensitive to the phases φ_1 and φ_2, which we therefore set to zero. Likewise, the precise choice of the positions $\boldsymbol{\tau}_n$ only amounts to phase shifting the potential and does not influence the results.

[1] E. Morosan, H. W. Zandbergen, B. S. Dennis, J. W. G. Bos, Y. Onose, T. Klimczuk, A. P. Ramirez, N. P. Ong, and R. J. Cava, Superconductivity in Cu_xTiSe_2, Nat. Phys. **2**, 544 (2006).

[2] B. Sipos, A. F. Kusmartseva, A. Akrap, H. Berger, L. Forró, and E. Tutis, From Mott state to superconductivity in 1T-TaS_2, Nat. Mater. **7**, 960 (2008).

[3] J. Chang, E. Blackburn, A. T. Holmes, N. B. Christensen, J. Larsen, J. Mesot, R. Liang, D. A. Bonn, W. N. Hardy, A. Watenphul, M. V. Zimmermann, E. M. Forgan, and S. M. Hayden, Direct observation of competition between superconductivity and charge density wave order in $YBa_2Cu_3O_{6.67}$, Nat. Phys. **8**, 871 (2012).

[4] G. Ghiringhelli, M. Le Tacon, M. Minola, S. Blanco-Canosa, C. Mazzoli, N. B. Brookes, G. M. De Luca, A. Frano, D. G. Hawthorn, F. He, T. Loew, M. Moretti Sala, D. C. Peets, M. Salluzzo, E. Schierle, R. Sutarto, G. A. Sawatzky, E. Weschke, B. Keimer, and L. Braicovich, Long-range incommensurate charge fluctuations in (Y,Nd)$Ba_2Cu_3O_{6+x}$, Science **337**, 821 (2012).

[5] Y. Y. Peng, R. Fumagalli, Y. Ding, M. Minola, S. Caprara, D. Betto, M. Bluschke, G. M. De Luca, K. Kummer, E. Lefrançois, M. Salluzzo, H. Suzuki, M. Le Tacon, X. J. Zhou, N. B. Brookes, B. Keimer, L. Braicovich, M. Grilli, and G. Ghiringhelli, Re-entrant charge order in overdoped

$(Bi,Pb)_{2.12}Sr_{1.88}CuO_{6+\delta}$ outside the pseudogap regime, Nat. Mater. **17**, 697 (2018).

[6] R. Comin, A. Frano, M. M. Yee, Y. Yoshida, H. Eisaki, E. Schierle, E. Weschke, R. Sutarto, F. He, A. Soumyanarayanan, Y. He, M. L. Tacon, I. S. Elfimov, J. E. Hoffman, G. A. Sawatzky, B. Keimer, and A. Damascelli, Charge order driven by fermi-arc instability in $Bi_2Sr_{2-x}La_xCuO_{6+d}$, Science **343**, 390 (2014).

[7] E. H. da Silva Neto, R. Comin, F. He, R. Sutarto, Y. Jiang, R. L. Greene, G. A. Sawatzky, and A. Damascelli, Charge ordering in the electron-doped superconductor $Nd_{2-x}Ce_xCuO_4$, Science **347**, 282 (2015).

[8] E. H. da Silva Neto, B. Yu, M. Minola, R. Sutarto, E. Schierle, F. Boschini, M. Zonno, M. Bluschke, J. Higgins, Y. Li, G. Yu, E. Weschke, F. He, M. L. Tacon, R. L. Greene, M. Greven, G. A. Sawatzky, B. Keimer, and A. Damascelli, Doping-dependent charge order correlations in electron-doped cuprates, Sci. Adv. **2**, e1600782 (2016).

[9] T. Valla, P. D. Johnson, Z. Yusof, B. Wells, Q. Li, S. M. Loureiro, R. J. Cava, M. Mikamik, Y. Morik, M. Yoshimura, and T. Sasakik, Coherence-incoherence and dimensional crossover in layered strongly correlated metals, Nature (London) **417**, 627 (2002).

[10] M. Hepting, L. Chaix, E. W. Huang, R. Fumagalli, Y. Y. Peng, B. Moritz, K. Kummer, N. B. Brookes, W. C. Lee, M. Hashimoto, T. Sarkar, J. F. He, C. R. Rotundu, Y. S. Lee, R. L. Greene, L. Braicovich, G. Ghiringhelli, Z. X. Shen, T. P. Devereaux, and W. S. Lee, Three-dimensional collective charge excitations in electron-doped copper oxide superconductors, Nature (London) **563**, 374 (2018).

[11] X. Xi, L. Zhao, Z. Wang, H. Berger, L. Forró, J. Shan, and K. F. Mak, Strongly enhanced charge-density-wave order in monolayer $NbSe_2$, Nat. Nanotechnol. **10**, 765 (2015).

[12] M. M. Ugeda, A. J. Bradley, Y. Zhang, S. Onishi, Y. Chen, W. Ruan, C. Ojeda-aristizabal, H. Ryu, M. T. Edmonds, H.-Z. Tsai, A. Riss, S.-K. Mo, D. Lee, A. Zettl, Z. Hussain, Z.-X. Shen, and M. F. Crommie, Characterization of collective ground states in single-layer $NbSe_2$, Nat. Phys. **12**, 92 (2016).

[13] F. Weber, R. Hott, R. Heid, L. L. Lev, M. Caputo, T. Schmitt, and V. N. Strocov, Three-dimensional Fermi surface of 2H-$NbSe_2$: Implications for the mechanism of charge density waves, Phys. Rev. B **97**, 235122 (2018).

[14] P. Chen, Y.-H. Chan, M.-H. Wong, X.-Y. Fang, M. Y. Chou, S.-K. Mo, Z. Hussain, A.-V. Federov, and T.-C. Chiang, Dimensional effects on the charge density waves in ultrathin films of $TiSe_2$, Nano. Lett. **16**, 6331 (2016).

[15] E. Navarro-Moratalla, J. O. Island, S. Mañas-Valero, E. Pinilla-Cienfuegos, A. Castellanos-Gomez, J. Quereda, G. Rubio-Bollinger, L. Chirolli, J. A. Silva-Guillén, N. Agrait, G. A. Steele, F. Guinea, H. S. J. van der Zant, and E. Coronado, Enhanced superconductivity in atomically thin TaS_2, Nat. Commun. **7**, 11043 (2016).

[16] A. K. Geim and I. V. Grigorieva, Van der Waals heterostructures, Nature (London) **499**, 419 (2013).

[17] K. S. Novoselov, A. Mishchenko, A. Carvalho, and A. H. Castro Neto, 2D materials and van der Waals heterostructures, Science **353**, aac9439 (2016).

[18] D. Jariwala, T. Marks, and M. C. Hersam, Mixed-dimensional van der Waals heterostructures, Nat. Mater. **16**, 170 (2016).

[19] P. Sessi, D. D. Sante, A. Szczerbakow, F. Glott, S. Wilfert, H. Schmidt, T. Bathon, P. Dziawa, M. Greiter, T. Neupert, G. Sangiovanni, T. Story, R. Thomale, and M. Bode, Robust spin-polarized midgap states at step edges of topological crystalline insulators, Science **354**, 1269 (2016).

[20] Y. Ma, H. C. Diaz, J. Avila, C. Chen, V. Kalappattil, R. Das, M.-H. Phan, T. Čadež, J. M. P. Carmelo, M. C. Asensio, and M. Batzill, Angle resolved photoemission spectroscopy reveals spin charge separation in metallic $MoSe_2$ grain boundary, Nat. Commun. **8**, 14231 (2017).

[21] A. S. Ngankeu, S. K. Mahatha, K. Guilloy, M. Bianchi, C. E. Sanders, K. Hanff, K. Rossnagel, J. A. Miwa, C. B. Nielsen, M. Bremholm, and P. Hofmann, Quasi-one-dimensional metallic band dispersion in the commensurate charge density wave of 1T-TaS_2, Phys. Rev. B **96**, 195147 (2017).

[22] E. Martino, A. Pisoni, L. Ćirić, A. Arakcheeva, H. Berger, A. Akrap, C. Putzke, P. J. W. Moll, I. Batistić, E. Tutiš, L. Forró, and K. Semeniuk, Preferential out-of-plane conduction and quasi-one-dimensional electronic states in layered van der Waals material 1T-TaS_2, arXiv:1910.03817.

[23] N. P. Ong and P. Monceau, Anomalous transport properties of a linear-chain metal: $NbSe_3$, Phys. Rev. B **16**, 3443 (1977).

[24] J. L. Hodeau, M. Marezio, C. Roucau, R. Ayroles, A. Meerschaut, J. Rouxel, and P. Monceau, Charge-density waves in $NbSe_3$ at 145 K : crystal structures, X-ray and electron diffraction studies, J. Phys. C: Solid State Phys. **11**, 4117 (1978).

[25] R. M. Fleming, D. E. Moncton, and D. B. McWhan, X-ray scattering and electric field studies of the sliding mode conductor $NbSe_3$, Phys. Rev. B **18**, 5560 (1978).

[26] C. Brun, Z. Z. Wang, and P. Monceau, Scanning tunneling microscopy at the $NbSe_3$ surface: Evidence for interaction between q_1 and q_2 charge density waves in the pinned regime, Phys. Rev. B **80**, 045423 (2009).

[27] F. Devreux, ^{93}Nb NMR study of $NbSe_3$, J. Phys. **43**, 1489 (1982).

[28] J. H. Ross, Z. Wang, and C. P. Slichter, NMR Study of the Structure and Motion of Charge Density Waves in $NbSe_3$, Phys. Rev. Lett. **56**, 663 (1986).

[29] S. van Smaalen, J. L. de Boer, A. Meetsma, H. Graafsma, H.-S. Sheu, A. Darovskikh, P. Coppens, and F. Levy, Determination of the structural distortions corresponding to the q_1- and q_2-type modulations in $NbSe_3$, Phys. Rev. B **45**, 3103 (1992).

[30] E. Canadell, I. E. Rachidi, J. P. Pouget, P. Gressier, A. Meerschaut, J. Rouxel, D. Jung, M. Evain, and M. H. Whangbo, Comparison of the electronic structures of layered transition-metal trichalcogenides $TaSe_3$, TaS_3, and $NbSe_3$, Inorg. Chem. **29**, 1401 (1990).

[31] S. Rouzière, S. Ravy, J. P. Pouget, and R. E. Thorne, X-ray investigation of the critical q_2-charge density wave fluctuations of $NbSe_3$, Solid State Commun. **97**, 1073 (1996).

[32] J. Schäfer, E. Rotenberg, S. D. Kevan, P. Blaha, R. Claessen, and R. E. Thorne, High-Temperature Symmetry Breaking in the Electronic Band Structure of the Quasi-One-Dimensional Solid $NbSe_3$, Phys. Rev. Lett. **87**, 196403 (2001).

[33] J. Schäfer, M. Sing, R. Claessen, E. Rotenberg, X. J. Zhou, R. E. Thorne, and S. D. Kevan, Unusual Spectral Behavior of Charge-Density Waves with Imperfect Nesting in a Quasi-One-Dimensional Metal, Phys. Rev. Lett. **91**, 066401 (2003).

[34] C. W. Nicholson, C. Berthod, M. Puppin, H. Berger, M. Wolf, M. Hoesch, and C. Monney, Dimensional Crossover in a Charge Density Wave Material Probed by Angle-Resolved Photoemission Spectroscopy, Phys. Rev. Lett. **118**, 206401 (2017).

[35] M. A. Valbuena, P. Chudzinski, S. Pons, S. Conejeros, P. Alemany, E. Canadell, H. Berger, E. Frantzeskakis, J. Avila, M. C. Asensio, T. Giamarchi, and M. Grioni, Polarization dependence of angle-resolved photoemission with submicron spatial resolution reveals emerging one-dimensionality of electrons in $NbSe_3$, Phys. Rev. B **99**, 075118 (2019).

[36] H. Requardt, J. E. Lorenzo, P. Monceau, R. Currat, and M. Krisch, Dynamics in the charge-density-wave system $NbSe_3$ using inelastic x-ray scattering with meV energy resolution, Phys. Rev. B **66**, 214303 (2002).

[37] H. Haifeng and Z. Dianlin, Charge Density Wave Gap Formation of $NbSe_3$ Detected by Electron Tunneling, Phys. Rev. Lett. **82**, 811 (1999).

[38] A. H. Moudden, J. D. Axe, P. Monceau, and F. Levy, q_1 Charge-Density Wave in $NbSe_3$, Phys. Rev. Lett. **65**, 223 (1990).

[39] C. Brun, Z.-Z. Wang, P. Monceau, and S. Brazovskii, Surface Charge Density Wave Phase Transition in $NbSe_3$, Phys. Rev. Lett. **104**, 256403 (2010).

[40] J. E. Lorenzo, R. Currat, P. Monceau, B. Hennion, H. Berger, and F. Levy, A neutron scattering study of the quasi-one-dimensional conductor $(TaSe_4)_2I$, J. Phys.: Condens. Matter **10**, 5039 (1998).

[41] J. A. Wilson, Bands, bonds, and charge-density waves in the $NbSe_3$ family of compounds, Phys. Rev. B **19**, 6456 (1979).

[42] H. Iwasawa, E. F. Schwier, M. Arita, A. Ino, H. Namatame, M. Taniguchi, Y. Aiura, and K. Shimada, Development of laser-based scanning μ-ARPES system with ultimate energy and momentum resolutions, Ultramicroscopy **182**, 85 (2017).

[43] T. Ozaki, Variationally optimized atomic orbitals for large-scale electronic structures, Phys. Rev. B **67**, 155108 (2003).

[44] T. Ozaki and H. Kino, Numerical atomic basis orbitals from H to Kr, Phys. Rev. B **69**, 195113 (2004).

[45] T. Ozaki and H. Kino, Efficient projector expansion for the *ab initio* LCAO method, Phys. Rev. B **72**, 045121 (2005).

[46] K. Lejaeghere, G. Bihlmayer, T. Björkman, P. Blaha, S. Blügel, V. Blum, D. Caliste, I. E. Castelli, S. J. Clark, A. D. Corso, S. D. Gironcoli, T. Deutsch, J. K. Dewhurst, I. D. Marco, C. Draxl, M. Du, O. Eriksson, J. A. Flores-livas, K. F. Garrity, L. Genovese *et al.* Reproducibility in density functional theory calculations of solids, Science **351**, aad3000 (2016).

[47] J. P. Perdew, K. Burke, and M. Ernzerhof, Generalized Gradient Approximation Made Simple, Phys. Rev. Lett. **77**, 3865 (1996).

[48] P. Blaha, K. Schwarz, G. Madsen, D. Kvasnicka, and J. Luitz, *An Augmented Plane Wave Plus Local Orbitals Program for Calculating Crystal Properties* (Techn. Universität Wien, Vienna, 2001).

[49] Z. Dai, C. G. Slough, and R. V. Coleman, Charge-density-wave modifications in $NbSe_3$ produced by Fe and Co doping, Phys. Rev. B **45**, 9469 (1992).

[50] K. Rossnagel, On the origin of charge-density waves in select layered transition-metal dichalcogenides, J. Phys.: Condens. Matter **23**, 213001 (2011).

[51] U. Chatterjee, J. Zhao, M. Iavarone, R. D. Capua, J. P. Castellan, G. Karapetrov, C. D. Malliakas, M. G. Kanatzidis, H. Claus, J. P. C. Ruff, F. Weber, J. V. Wezel, J. C. Campuzano, R. Osborn, M. Randeria, N. Trivedi, M. R. Norman, and S. Rosenkranz, Emergence of coherence in the charge-density wave state of 2H-$NbSe_2$, Nat. Commun. **6**, 6313 (2015).

[52] T. Yokoya, T. Kiss, A. Chainani, S. Shin, and K. Yamaya, Role of charge-density-wave fluctuations on the spectral function in a metallic charge-density-wave system, Phys. Rev. B **71**, 140504(R) (2005).

[53] M. Hoesch, L. Gannon, K. Shimada, B. J. Parrett, M. D. Watson, T. K. Kim, X. Zhu, and C. Petrovic, Disorder Quenching of the Charge Density Wave in $ZrTe_3$, Phys. Rev. Lett. **122**, 017601 (2019).

[54] A. Kanigel, U. Chatterjee, M. Randeria, M. R. Norman, G. Koren, K. Kadowaki, and J. C. Campuzano, Evidence for Pairing above the Transition Temperature of Cuprate Superconductors from the Electronic Dispersion in the Pseudogap Phase, Phys. Rev. Lett. **101**, 137002 (2008).

[55] C. W. Nicholson, A. Lücke, W. G. Schmidt, M. Puppin, L. Rettig, R. Ernstorfer, and M. Wolf, Beyond the molecular movie: Dynamics of bands and bonds during a photoinduced phase transition, Science **362**, 821 (2018).

[56] F. Wang, J. V. Alvarez, S. K. Mo, J. W. Allen, G. H. Gweon, J. He, R. Jin, D. Mandrus, and H. Höchst, New Luttinger-Liquid Physics from Photoemission on $Li_{0.9}Mo_6O_{17}$, Phys. Rev. Lett. **96**, 196403 (2006).

[57] C. Blumenstein, J. Schäfer, S. Mietke, S. Meyer, A. Dollinger, M. Lochner, X. Y. Cui, L. Patthey, R. Matzdorf, and R. Claessen, Atomically controlled quantum chains hosting a Tomonaga-Luttinger liquid, Nat. Phys. **7**, 776 (2011).

[58] Y. Ohtsubo, J.-i. Kishi, K. Hagiwara, P. Le Fèvre, F. Bertran, A. Taleb-Ibrahimi, H. Yamane, S.-i. Ideta, M. Matsunami, K. Tanaka, and S.-i. Kimura, Surface Tomonaga-Luttinger-Liquid State on Bi/InSb (001), Phys. Rev. Lett. **115**, 256404 (2015).

[59] M. D. Watson, Y. Feng, C. W. Nicholson, C. Monney, J. M. Riley, H. Iwasawa, K. Refson, V. Sacksteder, D. T. Adroja, J. Zhao, and M. Hoesch, Multiband One-Dimensional Electronic Structure and Spectroscopic Signature of Tomonaga-Luttinger Liquid Behavior in $Kr_2Cr_3As_3$, Phys. Rev. Lett. **118**, 097002 (2017).

[60] J. Voit, Charge-spin separation and the spectral properties of Luttinger liquids, J. Phys.: Condens. Matter **5**, 8305 (1993).

[61] J. Voit, One-dimensional Fermi liquids, Rep. Prog. Phys. **58**, 977 (1995).